Numerical modelling of the mechanical reliability of multicoated nano-encapsulated phase change materials with improved thermal performance

*Josep Forner-Escrig Nuria Navarrete Roberto Palma Damiano La Zara Aristeidis Goulas David Valdesueiro J. Ruud van Ommen Leonor Hernández Rosa Mondragón**

Josep Forner-Escrig, Nuria Navarrete, Leonor Hernández, Rosa Mondragón
Department of Mechanical Engineering and Construction, Universitat Jaume I, Av. de Vicent Sos Baynat, s/n 12071 Castelló de la Plana, Spain
Email Address: mondragn@uji.es
Roberto Palma
Department of Structural Mechanics and Hydraulic Engineering, University of Granada, Campus Universitario Fuentenueva, Edf. Politécnico, 18071 Granada, Spain
Damiano La Zara, Aristeidis Goulas, J. Ruud van Ommen
Department of Chemical Engineering, Delft University of Technology, 2629 HZ, Delft, the Netherlands
David Valdesueiro
Delft IMP B.V, Molengraaffsingel 10, 2629 JD, Delft, the Netherlands

Keywords: *Monte Carlo, Finite Element Method, Mechanical reliability, Nano-encapsulated phase change materials, Thermal energy storage*

Nano-encapsulated phase change materials (nePCMs), were investigated for enhancing thermal energy storage. However, the shell of these nanocapsules may fail due to stress developed during thermal processes, leading to melting enthalpy loss. To overcome this problem, SiO_2 and Al_2O_3 coatings on Sn nanoparticles were synthesised by atomic layer deposition (ALD). To study the influence of shell thickness and composition on the probability of failure (POF) of nePCM shells in single- and multicoated nePCMs, a probabilistic numerical tool combining Monte Carlo techniques and a thermo-mechanical finite element model with phase change was used. The uncertainties of the material and geometrical properties of nePCMs were included in the analysis. Both deterministic and probabilistic failure criteria were taken into account to consider the effect of dispersion on tensile strength. The results indicated that multicoated nePCMs enhanced thermo-mechanical performance in relation to their single-coated counterparts. Both the numerical simulations and experiments confirmed that the POF of nePCM shells and melting enthalpy loss in multicoated nePCMs lowered with shell thickness. The results after 50 ALD cycles indicated that Al_2O_3 coatings exhibited better performance because a POF of 1.66% was obtained with 1.1% enthalpy loss, while the POF for SiO_2 was 72.38% with 3.5% enthalpy loss.

1 Introduction

One of the most active research fields today is energy conversion, which forms part of energy transition from conventional energy sources to renewable energies. From the wide variety of existing renewable energies, solar energy is worthy of special mention because it represents a massive reliable energy source. More specifically, and according to the International Energy Agency[1], it is estimated that the Sun takes a little more than 2 hours to send the necessary amount of energy to meet our planet's annual energy needs by 2035. However, one of the main drawbacks of solar energy is that energy generation is subjected to weather/climate conditions. This unpredictability may bring about a mismatch between energy demand and supply, which might entail instability issues for the electrical grid's operation. For this reason, thermal energy storage (TES) systems are particularly important.
In the solar thermal energy context, nanofluids based on molten salts are one of the technologies being studied for TES purposes in concentrated solar power (CSP) plants[2]. Nanofluids consist of solid nanosized particles dispersed in a base fluid[3]. Their ability to store energy traditionally relied on their sensible storage capability, which is limited by the heat capacity and temperature difference undergone by the storage medium. More recently, phase change materials (PCMs) have been used as the solid component of nanofluids to boost their energy storage capability by means of the contribution of latent heat storage[4–11]. However, to prevent these PCMs from leaking when molten, they need to be confined within a shell made of a material with a higher melting point than the PCM core. If PCMs fall within the nanometric size range, they are called nano-encapsulated PCMs (nePCMs). Normally, metallic nanoparticles

(NPs) are self-encapsulated by a native oxide layer formed by passivation (metal@metal_oxide), which is not always sufficient to avoid the leakage of nePCMs' molten core[12,13].
When going through thermal processes, nanofluids containing nePCMs tend to partially or totally lose nePCM phase change enthalpy. nePCM shell mechanical failure due to stress arising during thermal processes has been proposed as one of the causes of such enthalpy loss[12,14–16]. Recently, a solution put forward to overcome this issue consisted in creating a multicoated nePCM by synthesising a second shell by the cutting-edge technique of atomic layer deposition (ALD)[17]. This technique involves the cyclical exposure of self-encapsulated nePCMs to two different gas precursors that chemisorb on the available nePCM surface for it to grow an additional inorganic shell with thickness control at the subnanometer level by tuning the number of cycles[18]. The ALD of nanoscale layers of SiO_2 and Al_2O_3 allowed the thermal energy storage of nePCMs to improve by reducing cores' enthalpy loss.
The main challenge in the synthesis of single- and multicoated nePCMs lies in determining the optimal shell thickness that confines nePCM cores because a compromise between mechanical reliability and energy storage has to be reached, which can contribute to reduce the coating cost of nePCMs and to gain control over the colloidal stability of nanofluids. Increasing the shell thickness of nePCMs enhances the shell's mechanical strength but reduces the energy storage density of nePCMs as the shell material does not contribute to latent heat storage. Besides, increasing the overall nePCM size to enhance the energy density capability of a nanofluid may jeopardise its colloidal stability and cause particles to settle. Therefore, understanding the reasons for nePCM shell mechanical failure is necessary. In this vein, a thermo-mechanical finite element (FE) model with phase change was developed in a previous work[19] to predict nePCM shell failure during thermal processes. Experimental measurements and the characterisation of nePCMs are not exempt of uncertainties, which are intrinsically related to the nature of the measurement process. Therefore, it is of crucial importance to verify the influence that dispersion in material properties and geometrical parameters of nePCMs can have on their mechanical reliability. The consideration of these uncertainties demonstrates the need to adopt a probabilistic numerical tool to predict nePCM behaviour, as shown in the literature[20,21]. For this reason, the thermo-mechanical phase change FE model is combined with Monte Carlo (MC) techniques, a class of algorithms that use statistically generated samples to approach the solution of a model in a probabilistic sense. These samples are the model's input and outputs are obtained by evaluating the FE model.
The objective of the present work is to study two parameters: the mechanical reliability of multicoated nePCMs and their enthalpy loss to analyse the effect of adding a second nano-encapsulating coating, the influence of its thickness on both parameters, and the possible relation between them. Coatings were experimentally synthesised to obtain multicoated (core@inner_shell@outer_shell materials) nePCMs: $Sn@SnO_2@SiO_2$ and $Sn@SnO@Al_2O_3$[17]. The experimental characterisation of the multicoated nePCMs was performed in an N_2 atmosphere to be able to rule out oxidation as the cause of nePCM cores' enthalpy loss. In that case, the core's enthalpy loss could only be explained by the nePCM shell mechanical failure. To fulfil this aim, the probabilistic tool that combined MC methods and the FE thermo-mechanical model was used. For the numerical simulations, 30 random variables were defined to characterise the behaviour of the multicoated nePCMs and samples were generated by the Latin Hypercube Sampling (LHS) technique[22]. For the reliability analysis, both deterministic and probabilistic failure criteria were considered to also account for the influence of dispersion on the tensile strength of the materials forming nePCM shells, while Rankine's criterion was applied to compute the equivalent stress in these shells. Finally, and according to both experimental results and numerical predictions, the agreement observed between nePCM cores' enthalpy loss and the probability of failure (POF) of their shells could be used to validate the numerical tool.

2 Materials and Methods

2.1 Materials

Commercial Sn nanoparticles of nominal size <300 nm were purchased from US Research Nanomaterials, Inc. These nanoparticles were produced by the electro-physical fumed combined with the strong airflow

injection method, and were morphologically, chemically and thermally characterised in previous studies[12,17]. The experimental results showed self-encapsulated Sn@SnO nePCMs with a mean diameter of 180 nm.

Regarding the ALD process, the Al precursor, trimethylaluminum (TMA), was purchased from Akzo Nobel HPMO in a 600 mL stainless steel bubbler canister. The Si precursor, silicon tetrachloride ($SiCl_4$), was supplied by Sigma-Aldrich. Demineralised water was used as a coreactant for both SiO_2 and Al_2O_3 ALD. All the precursors were contained in stainless steel bubblers and used as received.

Coatings were synthesised by ALD in a fluidised bed reactor[23] starting from Sn@SnO nePCMs to obtain two different multicoated nePCMs: $Sn@SnO_2@SiO_2$ and $Sn@SnO@Al_2O_3$ after 5, 25 and 50 ALD cycles. Table 1 shows the evolution of the multicoated nePCMs' shell thickness with a rising number of ALD cycles. These shell thickness values employed herein were calculated from the values of growth per cycle (GPC) reported in the work by Navarrete et al.[17] by assuming that the deposition rate was linear, as could be observed in the inductively coupled plasma mass spectrometry (ICP-OES) experimental tests performed in the previously mentioned work. Further details of the characterisation of nePCMs and the synthesis of their coating by ALD are found in the same previous work[17]. It is noteworthy that the chemical characterisation of samples by X-ray diffraction confirmed that the tin oxide shell was initially amorphous, but became crystalline after being submitted to high temperature. However, the final crystalline phase differed depending on the outer shell (silica or alumina), probably due to the different arrangement of atoms and the further inner shell oxidation, influenced by the chemical and structural composition of the outer one, as confirmed by TGA in the previous reference.

Number of ALD cycles	**Shell thickness**	
	$Sn@SnO_2@SiO_2$	**$Sn@SnO@Al_2O_3$**
5	$e_{SnO_2} = 12$ nm $e_{SiO_2} = 0.8$ nm	$e_{SnO} = 12$ nm $e_{Al_2O_3} = 1$ nm
25	$e_{SnO_2} = 12$ nm $e_{SiO_2} = 4$ nm	$e_{SnO} = 12$ nm $e_{Al_2O_3} = 5$ nm
50	$e_{SnO_2} = 12$ nm $e_{SiO_2} = 8$ nm	$e_{SnO} = 12$ nm $e_{Al_2O_3} = 10$ nm

Table 1: Summary of shell thickness combinations in relation to the number of atomic layer deposition (ALD) cycles for $Sn@SnO_2@SiO_2$ and $Sn@SnO@Al_2O_3$ (core@inner_shell@outer_shell) nano-encapsulated phase change materials.

The Sn@SnO and multicoated $Sn@SnO_2@SiO_2$ and $Sn@SnO@Al_2O_3$ nePCMs synthesised by 50 ALD cycles were imaged by field emission transmission electron microscopy (TEM). In Figure 1, two distinct shells are clearly observed for each multicoated nePCM.

The material and geometrical properties of the tin (Sn)[24–28], tin(IV) oxide (SnO_2)[29–33], silica (SiO_2)[24,34–37] and alumina (Al_2O_3)[24,38–40] used for numerical simulation are reported in Tables 2 and 3. For the numerical simulation of Sn@SnO nePCMs, the data from core and inner shell in Table 3 were employed. For the geometry of nePCMs, a single three-dimensional multicoated ellipsoidal nePCM was considered to incorporate the effects of geometrical uncertainty into the present study because not all nePCMs are necessarily perfectly spherical.

The material properties listed in Tables 2 and 3 are mass density ρ, specific heat capacity c, thermal conductivity κ, Young's modulus E, Poisson's ratio ν, thermal expansion coefficient α, melting temperature T_m and latent heat L. Subscripts s and l denote the solid state and the liquid state, respectively. Variables a_{semi}, b_{semi} and c_{semi} refer to the three outer semi-axes of an ellipsoidal nePCM and e_{shell} denotes shell thickness. Subscripts i and o indicate the inner shell and the outer shell, respectively.

In order to apply the MC techniques in the numerical analysis of the multicoated nePCMs, the model's input parameters (material and geometrical properties) were taken as random variables, whose nominal values and standard deviations (σ) in relation to their nominal values are found in Tables 2 and 3. Bear-

	Property	Values	Units	σ(%)
Core (Sn)	ρ_s	7280	kg/m^3	5
	ρ_l	6800	kg/m^3	5
	c_s	230	J/ (kg K)	5
	c_l	257	J/ (kg K)	5
	κ_s	65	W/ (m K)	5
	κ_l	31	W/ (m K)	5
	E	43.3	GPa	5
	ν	0.33	-	5
	α	2×10^{-5}	1/K	5
	T_m	498.65	K	5
	L	60.627	kJ/kg	5
Inner Shell (SnO_2)	ρ	7020	kg/m^3	5
	c	348.95	J/ (kg K)	5
	κ	40	W/ (m K)	5
	E	222.72	GPa	5
	ν	0.284	-	5
	α	4×10^{-6}	1/K	5
	T_m	1900	K	5
Outer Shell (SiO_2)	ρ	2200	kg/m^3	5
	c	962.86	J/ (kg K)	5
	κ	1.7	W/ (m K)	5
	E	75	GPa	5
	ν	0.17	-	5
	α	5.7×10^{-7}	1/K	5
	T_m	1986.15	K	5
Geometry	a_{semi}	90	nm	1
	b_{semi}	90	nm	1
	c_{semi}	90	nm	1
	$e_{shell,i}$	(*)	nm	1
	$e_{shell,o}$	(*)	nm	1

(*) See Table 1 for the shell thickness values, which depend on the number of ALD cycles.

Table 2: Summary of the material and geometrical properties of Sn@SnO_2@SiO_2 (core@inner_shell@outer_shell) nano-encapsulated phase change materials (nePCMs). σ is the standard deviation for each property in relation to their mean values.

	Property	Values	Units	σ(%)
Core (Sn)	ρ_s	7280	kg/m^3	5
	ρ_l	6800	kg/m^3	5
	c_s	230	J/ (kg K)	5
	c_l	257	J/ (kg K)	5
	κ_s	65	W/ (m K)	5
	κ_l	31	W/ (m K)	5
	E	43.3	GPa	5
	ν	0.33	-	5
	α	2×10^{-5}	1/K	5
	T_m	498.65	K	5
	L	60.627	kJ/kg	5
Inner Shell (SnO)	ρ	7020	kg/m^3	10
	c	348.95	J/ (kg K)	10
	κ	40	W/ (m K)	10
	E	222.72	GPa	10
	ν	0.284	-	10
	α	4×10^{-6}	1/K	10
	T_m	1900	K	10
Outer Shell (Al_2O_3)	ρ	3970	kg/m^3	5
	c	919.38	J/ (kg K)	5
	κ	10	W/ (m K)	5
	E	370	GPa	5
	ν	0.24	-	5
	α	8.2×10^{-6}	1/K	5
	T_m	2273.15	K	5
Geometry	a_{semi}	90	nm	1
	b_{semi}	90	nm	1
	c_{semi}	90	nm	1
	$e_{shell,i}$	(*)	nm	1
	$e_{shell,o}$	(*)	nm	1

(*) See Table 1 for the shell thickness values, which depend on the number of ALD cycles.

Table 3: Summary of the material and geometrical properties of Sn@SnO@Al_2O_3 (core@inner_shell@outer_shell) nano-encapsulated phase change materials (nePCMs). σ is the standard deviation for each property in relation to their mean values.

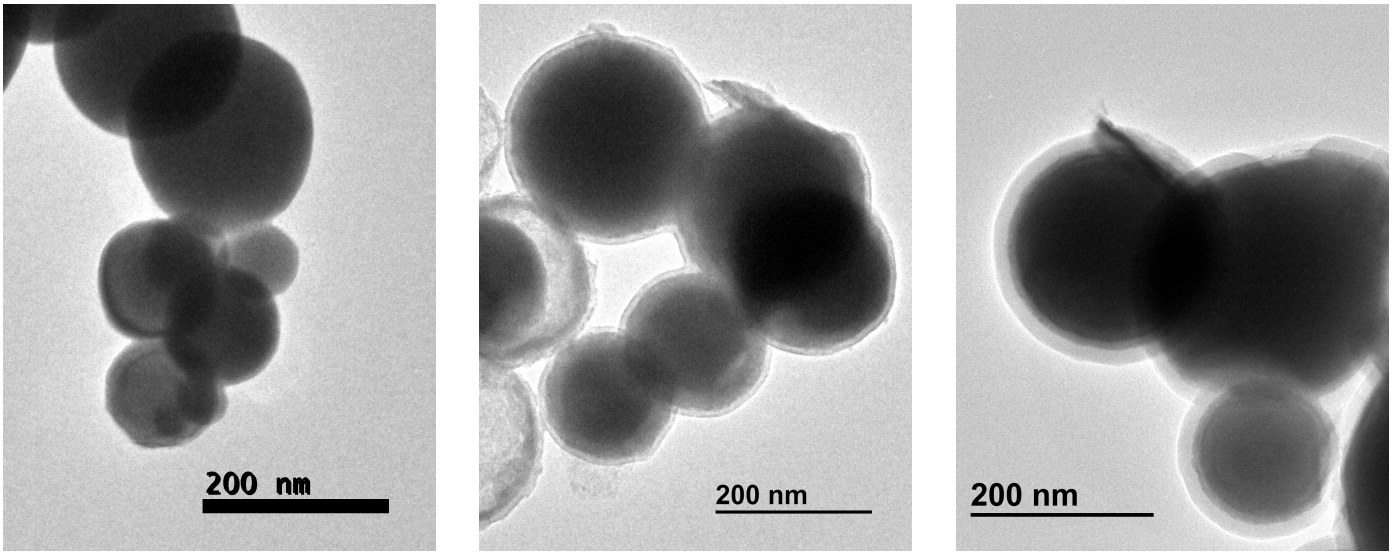

Figure 1: TEM images of Sn@SnO (left) and multicoated Sn@SnO_2@SiO_2 (centre) and Sn@SnO@Al_2O_3 (right) nePCMs synthesised by ALD technique after 50 cycles.

ing in mind the orders of magnitude in the measurement dispersion reported in the literature[24], a standard deviation of 5% was chosen as a good first approximation for errors in the material properties of Sn, SnO_2, Al_2O_3 and SiO_2 as the uncertainty values needed to perform the MC analysis. However, to the best of the authors' knowledge, the complete set of thermo-mechanical properties of SnO, required for the simulations with the present model, are not available in the literature. As both oxidation states of Sn possess a tetragonal crystallographic structure[41,42], material properties of SnO were considered to be obtained from the normal distribution of the SnO_2 material properties, but with a larger dispersion of 10%. In the present work, all material properties were assumed to be normally distributed, except for the size of nePCMs that follows log-normal distribution[12]. More precisely, the mean size of the outer semi-axes of nePCMs and its standard deviation were 90 nm and 40%, respectively.
Although experimentally observed nePCMs are not perfect spheres, their morphology does not significantly differ from particle to particle[17] and, therefore, a standard deviation of 1% around the log-normal mean values was considered. Furthermore, shell thickness was normally distributed with an uncertainty of 1% around its nominal value, which depended on the number of ALD cycles, as reported in Table 1. Finally, the nominal values of tensile strength σ_t considered for the reliability analysis were: 803, 110, 275.9 MPa for SnO_2[33], SiO_2[43] and Al_2O_3[39], respectively. For the probabilistic failure criterion, σ_t was assumed to be normally distributed with 20% dispersion around the nominal values.

3 Characterisation techniques

3.1 Thermogravimetric analysis, TGA

Thermal stability was studied for all the nePCMs by the thermogravimetric analysis (TGA). TGA 1 (Mettler Toledo) was used in an N_2 atmosphere. The temperature of each sample was left at 343 K for 5 min before being raised to 553 K at the 5 K/min rate, and held at 553 K for 30 min, while measuring all the changes in mass that took place. Approximately 20 mg of sample were placed inside a 40 µl aluminium crucible for each test.

3.2 Differential scanning calorimetry, DSC

Information about the melting enthalpies and temperatures of nePCMs was obtained by differential scanning calorimetry (DSC) (DSC2, Mettler Toledo). Samples of around 20 mg of nePCMs were analysed in a 40 µL aluminium crucible. Next, 80 thermal cycles from 343 K to 553 K were run in a nitrogen atmo-

sphere (25 mL/min N_2 flow rate), with 20 K/min heating and cooling rates and 5 min isotherms at maximum and minimum temperatures. More detailed analyses were performed every 10 cycles with the same characteristics, but at heating and cooling rates of 5 K/min to obtain more accurate values of enthalpies and temperatures.

4 Numerical tool

This section presents the details for the numerical analysis of the mechanical reliability of nePCMs.

4.1 Model description

In order to perform a reliability analysis and to incorporate the measurement uncertainties into the numerical model, a probabilistic tool was developed by combining a thermo-mechanical FE code and MC techniques and its flowchart is shown in Figure 2. For the FE model, meshes of 3584 and 5120 8-noded elements with 4 degrees of freedom (dofs) per node were defined for the single- and multicoated nePCMs, respectively.

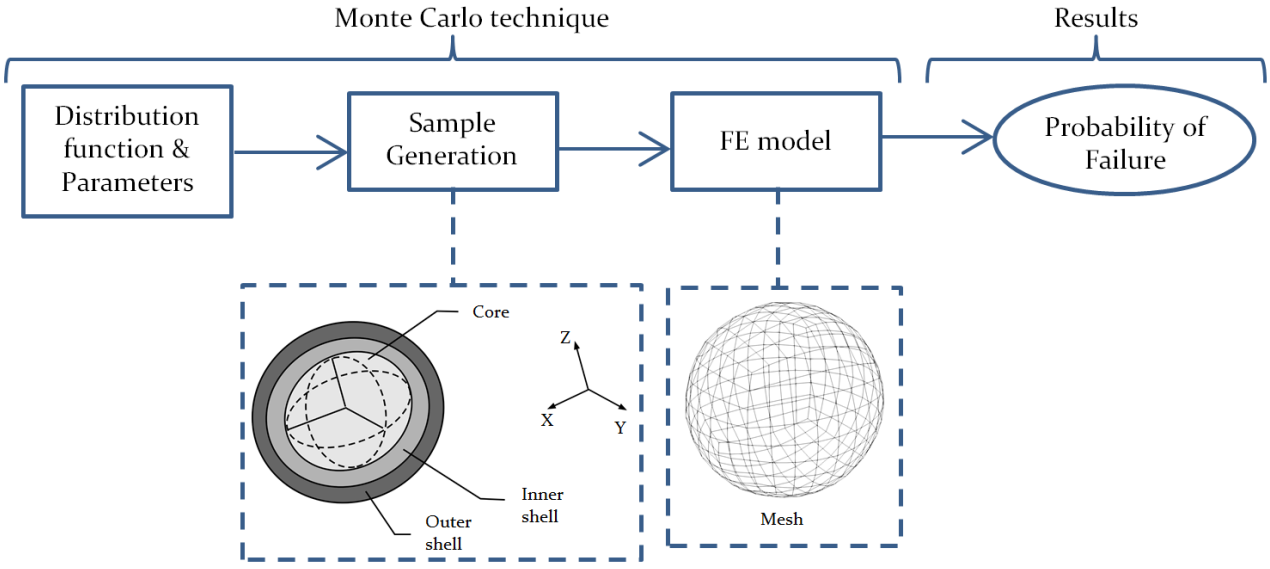

Figure 2: Flowchart of the probabilistic numerical tool.

Regarding the boundary and initial conditions, a nePCM is mechanically fixed at its centre and subjected to an initial temperature T_i. Then the prescribed temperature on the outer shell was linearly increased until a value T_0 (higher than the core's melting temperature) was obtained. In this case, T_i = 343.15 K and T_0 = 553.15 K were considered.

4.2 Probability of failure

The performance parameter retained for the analysis of nePCM's mechanical strength in the present work was their POF, which represents the frequency of occurrence of a given event tagged as failure which, in this case, corresponded to the frequency of neCPM shell mechanical failure. POF is mathematically defined as follows[44]:

$$\mathrm{POF} = P\left[G\left(\xi_j\right) \leq 0\right] = \int_{G(\xi_j)\leq 0} f_{\xi_j}\left(\Xi_j\right) \mathrm{d}\Xi_j, \tag{1}$$

where ξ_j, $f_{\xi_j}\left(\Xi_j\right)$ and $G\left(\xi_j\right)$ represent the vector of input random variables, the joint probability density function of the input random variables and a limit state function, respectively, and consequently, situations in which $G\left(\xi_j\right) \leq 0$ represent a violation of the limit state, i.e. the failure region. In general,

equation (1) cannot be analytically evaluated, but POF can be numerically computed. One of the techniques to numerically determine this POF is MC techniques and, according to Melchers and Beck[44], POF can be evaluated for these techniques as:

$$\text{POF} \approx \frac{n\left[G\left(\hat{\xi}_j \leq 0\right)\right]}{N}, \tag{2}$$

where $n\left[G\left(\hat{\xi}_j \leq 0\right)\right]$ is the number of cases n for which the limit state function is violated and N represents the number of MC iterations. In Equation (2), $\hat{\xi}_j$ is used to represent a sample value of the vector of input random variables.

5 Results

This section presents both the experimental and numerical results obtained for the Sn@SnO, Sn@SnO_2@SiO_2 and Sn@SnO@Al_2O_3 nePCMs.

5.1 Thermal stability

In order to test nePCMs' thermal stability, a TGA analysis in an N_2 atmosphere was performed on samples. Their behaviour when subjected to a progressive increase in temperature from 343 K to a posterior isotherm at 553 K is shown in Figure 3, where mass variations are observed.
At the beginning, the Sn@SnO nePCMs sample lost some mass, which likely corresponded to the impurities present in commercial nanoparticles, such as anti-agglomerant additives that are often added to industrially produced powders. Above 513 K however, the sample showed no weight variations, which indicates a completely stable behaviour at high temperatures.
A similar trend was observed for the multicoated nePCMs. With the Sn@SnO_2@SiO_2 samples, the initial weight loss was greater than for the Sn@SnO nePCMs. These mass losses were bigger for the multicoated nePCMs submitted to more ALD cycles and, therefore, they can be attributed to the presence of some residual products after ALD coating (namely chlorine compounds, as previously observed and reported by Navarrete et al.[17]), apart from the aforementioned impurities of commercial nanoparticles. Nevertheless, as previously noted for the Sn@SnO nePCMs, the Sn@SnO_2@SiO_2 samples also displayed thermally stable behaviour above 513 K, with only slight weight variations in the sample subjected to five ALD cycles, which was in any case below the 0.1% variation of total mass.
Regarding Sn@SnO@Al_2O_3 nePCMs, the initial mass losses were lower than in the other cases, which could also be explained by the impurities of commercial nanoparticles and ALD ligand leftovers (most likely carbonaceous species from TMA). As seen for Sn@SnO_2@SiO_2, after five ALD cycles nePCMs underwent a subtle mass increase (below 0.2%) when exposed to an isotherm of 553 K for 30 min, whereas the samples coated with 25 and 50 ALD cycles remained completely stable at this temperature.
In any case, the mass variations observed for all the analysed samples were lower than 1% variation of the total sample weight, which accounted for the good thermal stability of the multicoated Sn nePCMs. Moreover, as the thermal stability of samples was experimentally tested in an N_2 atmosphere, the mass fluctuations that occurred would not have been caused by oxidation.

5.2 Melting enthalpy and temperature

The stability of nePCMs to thermal cycling and the suitability of the different ALD coatings as a confining barrier for nePCMs' molten cores were tested in an N_2 atmosphere by subjecting samples to thermal DSC cycles up to 553 K. Figure 4 shows a zoom of the DSC curves obtained during the first melting DSC cycle for all the nePCM samples. The influence of the number of ALD cycles and, thus of shell thickness, was observed for the Sn@SnO_2@SiO_2 (Figure 4 a) and Sn@SnO@Al_2O_3 (Figure 4 b) samples, together with uncoated Sn@SnO (0 ALD cycles). From these curves, melting enthalpy (H_0) and temperat-

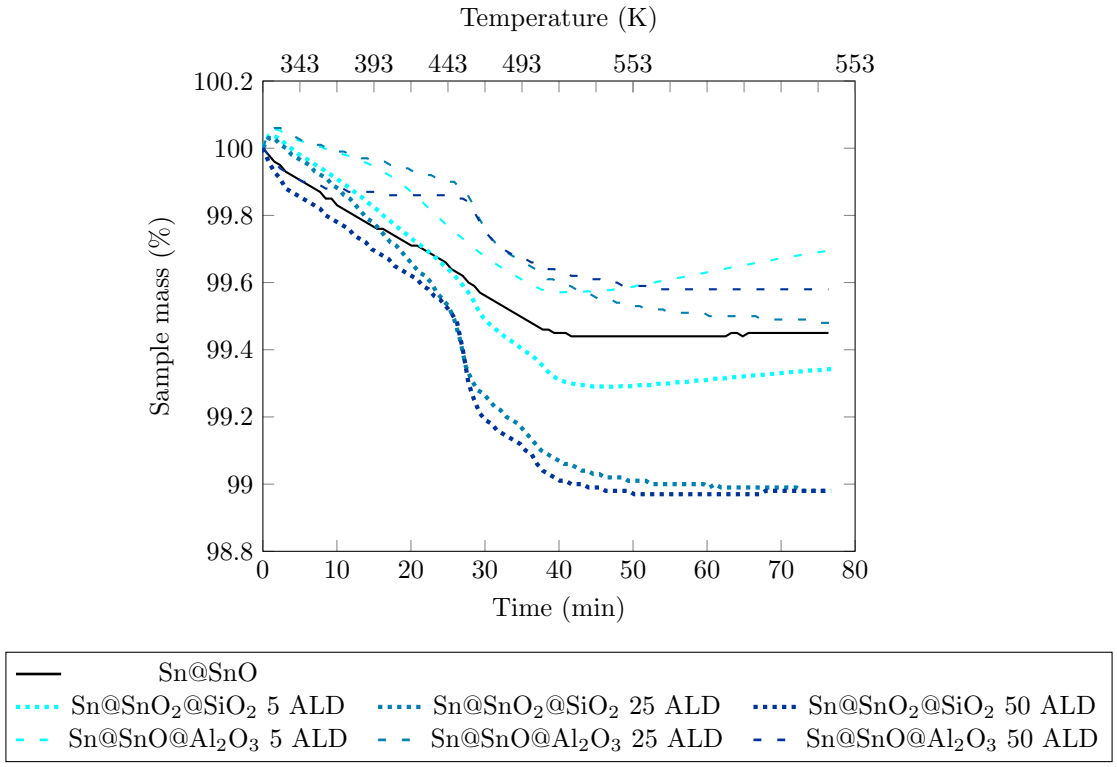

Figure 3: The TGA analysis of the Sn@SnO, Sn@SnO_2@SiO_2 and Sn@SnO@Al_2O_3 nano-encapsulated phase change materials subjected to different numbers of ALD cycles.

ure (T_m) were obtained for further analyses, and the initial values are shown in Table 4. It can be concluded that outer shell thickness did not influence the melting temperature for either silica or alumina coatings as expected from the low weight percentage of the shell components compared to the metal core.

Sample	**ALD cycles**	**Shell thickness (nm)**	H_0 **(kJ/kg)**	T_m **(K)**
Sn@SnO_2@SiO_2	0	0	52.71	505.15
	5	0.8	50.11	505.73
	25	4	51.74	505.28
	50	8	49.24	505.9
Sn@SnO@Al_2O_3	0	0	52.71	505.15
	5	1	52.26	507.44
	25	5	51.39	507.09
	50	10	51.74	506.14

Table 4: Influence of shell thickness on the initial melting enthalpy (H_0) and temperature (T_m).

Enthalpy evolution with the number of the thermal cycles is plotted in Figure 5 as the ratio between the melting enthalpy for the current cycle (H) and the initial enthalpy value (H_0), where both ALD-coated nePCMs showed greater thermal stability than the Sn@SnO nePCMs surrounded exclusively by the SnO layer. The decrease in the phase change enthalpy of the Sn@SnO nePCM, almost 7%, was notably reduced in both the Sn@SnO_2@SiO_2 and Sn@SnO@Al_2O_3 samples.
After 50 ALD cycles, the Sn@SnO@Al_2O_3 nePCMs exhibited the best resistance to enthalpy loss against thermal cycling by losing only a 1.1% of the initial melting enthalpy. In turn, the Sn@SnO_2@SiO_2 nePCMs showed greater melting enthalpy loss (3.5%) under the same conditions.

a) $Sn@SnO_2@SiO_2$

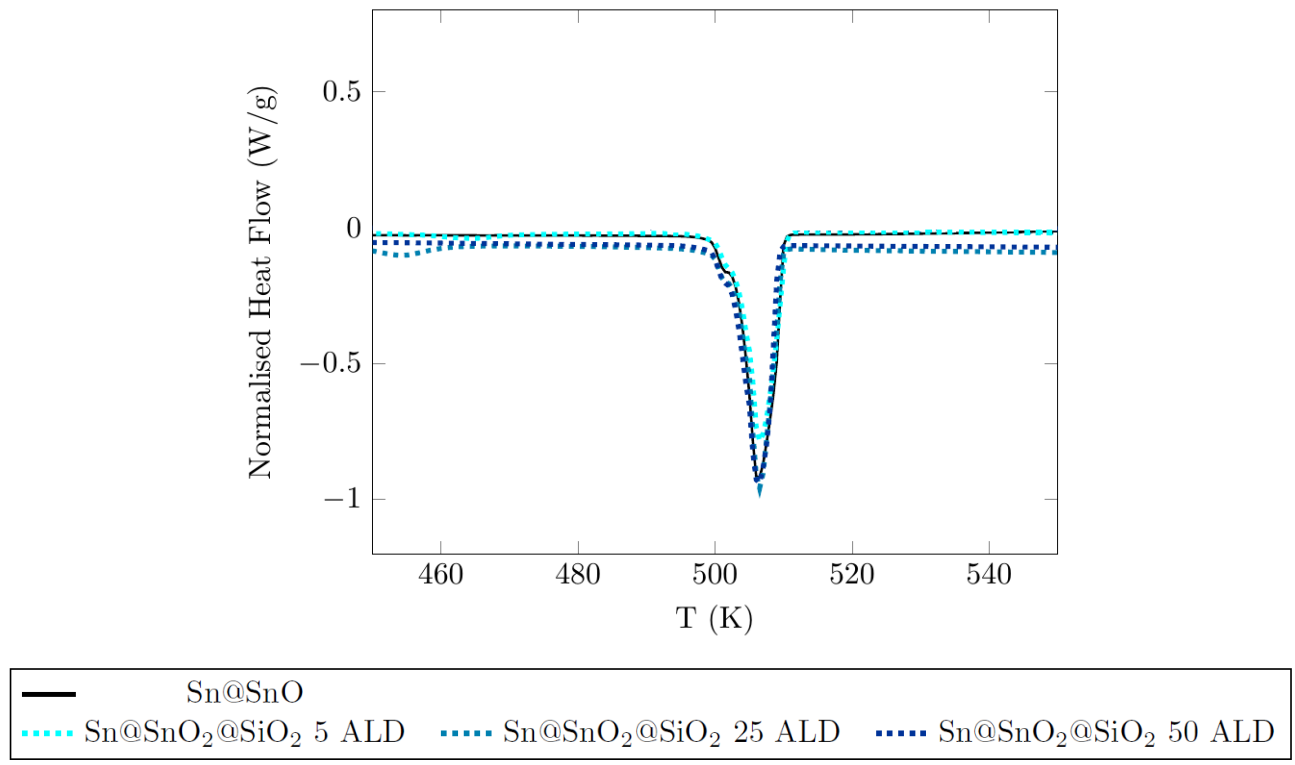

b) $Sn@SnO@Al_2O_3$

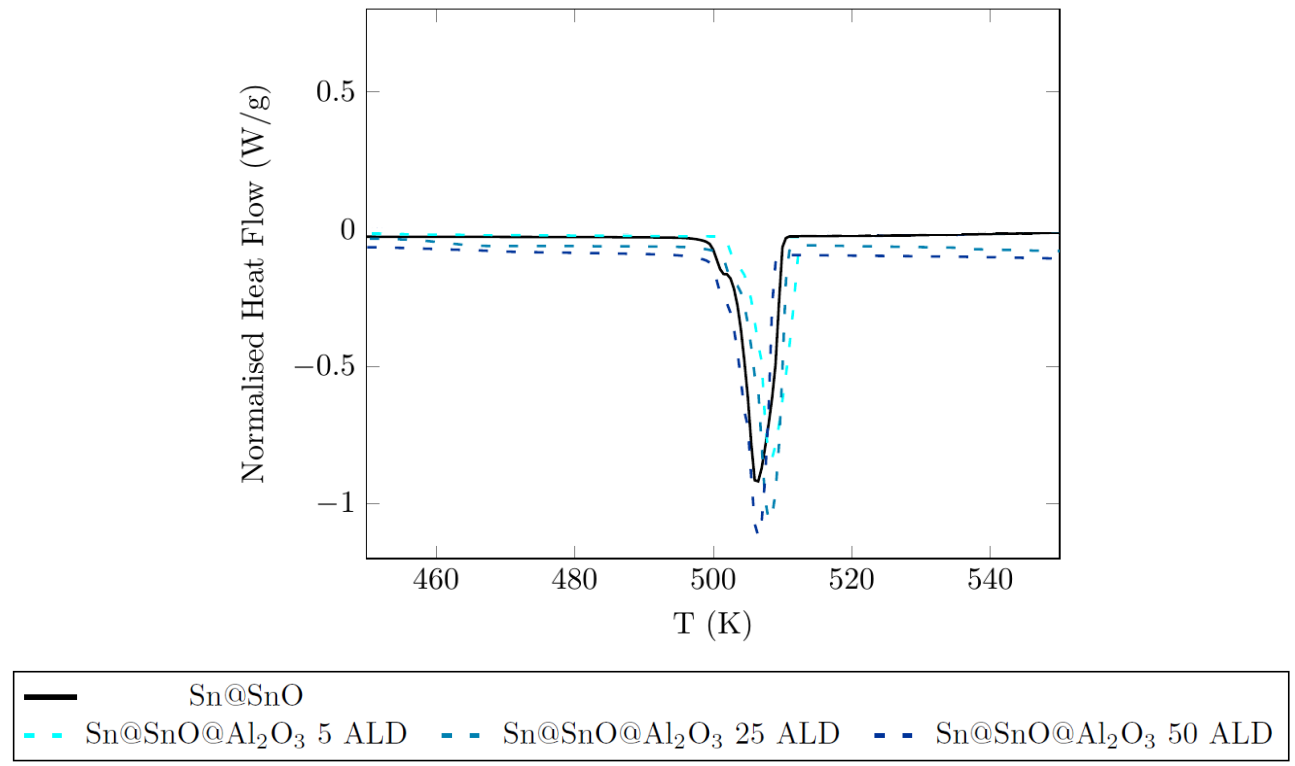

Figure 4: DSC curves of the first melting DSC cycle for the uncoated Sn@SnO and a) $Sn@SnO_2@SiO_2$ and b) $Sn@SnO@Al_2O_3$ nePCMs.

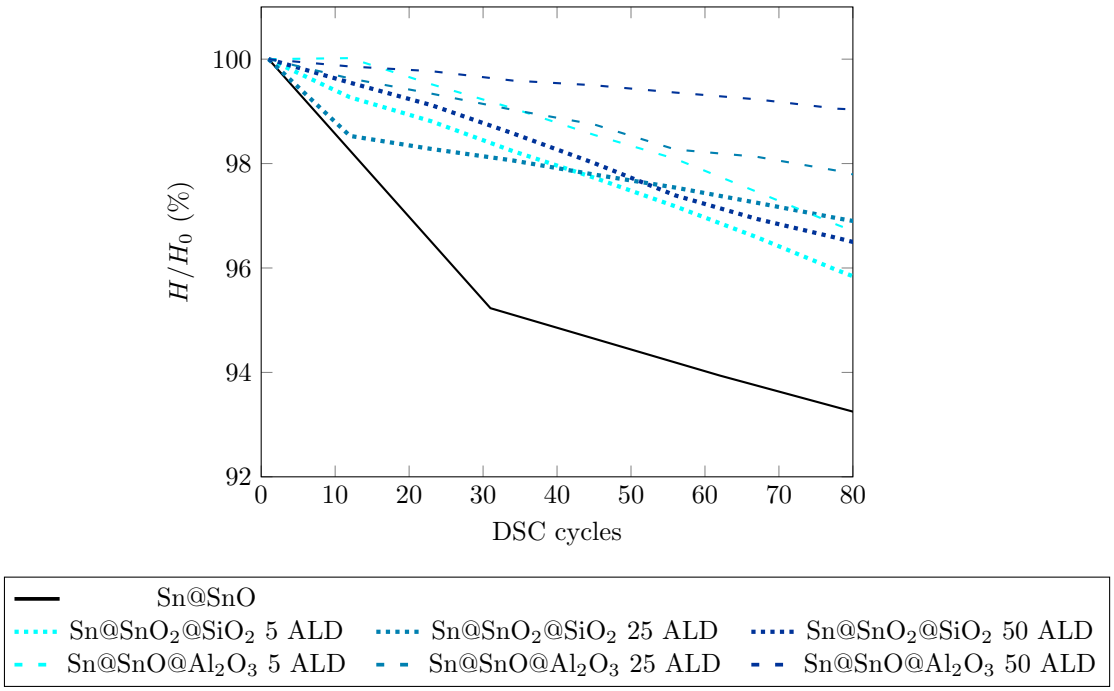

Figure 5: Evolution of melting enthalpy (H) in relation to the initial enthalpy value (H_0) with thermal cycling in a nitrogen (N_2) atmosphere for the Sn@SnO, Sn@SnO_2@SiO_2 and Sn@SnO@Al_2O_3 nePCMs subjected to different numbers of ALD cycles.

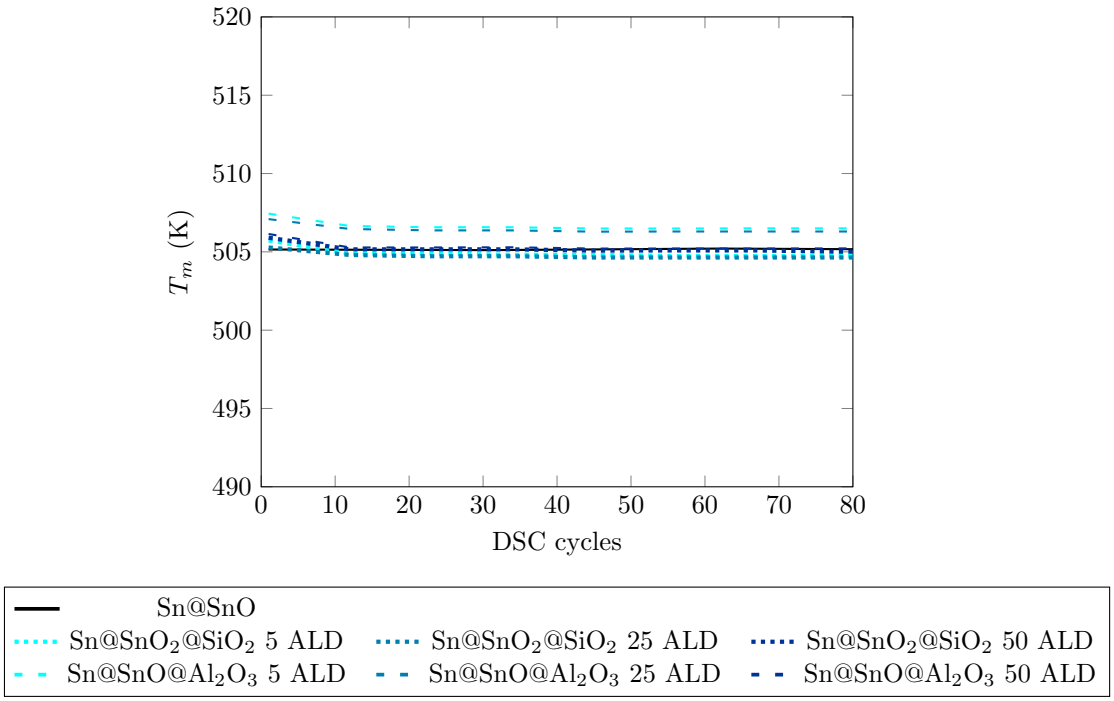

Figure 6: Evolution of the melting temperature (T_m) with thermal cycling in a nitrogen (N_2) atmosphere for the Sn@SnO, Sn@SnO_2@SiO_2 and Sn@SnO@Al_2O_3 nePCMs subjected to different numbers of ALD cycles.

Figure 6 shows the evolution of the melting temperature with thermal cycling. It can be observed that the transition temperature is constant and a maximum difference of 2.8 K was obtained among all the samples regardless of composition and shell thickness.
Therefore, the multicoated nePCMs coated with Al_2O_3 presented greater latent heat stability over cycles than their SiO_2 counterparts. This means better resistance to enthalpy loss, which implies better performance as a means for storing energy in nanofluids, while the phase change temperature remains unchanged. As the thermal characterisation of multicoated samples was performed in an N_2 atmosphere and, consequently, the TGA did not reveal any oxidation phenomena when the same thermal cycling was applied, nePCMs' enthalpy loss could have been due to the nePCM coating mechanical failure.

5.3 Probability of failure

Regarding the numerically calculated POF, Figure 7 shows the stress distribution for both the deterministic (left) and probabilistic (right) failure criteria for the Sn@SnO, Sn@SnO_2@ SiO_2 and Sn@SnO@Al_2O_3 nePCMs after 50 ALD cycles. POF values were obtained by comparing the overlapping between stress predictions (in blue in Figure 7) and the deterministic/probabilistic criteria (in red in Figure 7). For instance, for the Sn@SnO nePCMs, the equivalent stress distribution fell below the deterministic failure criterion. This means that the POF of Sn@SnO encapsulation was 0% when comparing the numerical predictions of the maximum equivalent stress to the deterministic value of tensile strength reported in the literature. However, the value provided by the probabilistic failure criterion for the Sn@SnO nePCMs was 2.27%. In this case, a probabilistic failure criterion allowed us to assess the nePCMs' mechanical performance by comparing the predicted maximum equivalent stress to a set of tensile strength values obtained from probability distribution. The same analysis performed for the multicoated nePCMs showed for the Sn@SnO_2@SiO_2 nePCMs after 50 ALD cycles that the deterministic POF of the outer shell was 73%, while the value provided by the probabilistic failure criterion was 72.38%. Finally for their Sn@SnO@Al_2O_3 counterparts, the deterministic POF of the outer shell was 0%, but was 1.66% for the probabilistic POF.
Therefore, these results stress the need to take into account probabilistic failure criteria because not considering them may slightly underestimate the mechanical POF of nePCM shells, which might have consequences on the nanofluid performance by reducing its effective energy storage capability if the number of nePCM failures exceeds that expected for an application. Furthermore, the use of a probabilistic criterion allows the number of necessary Monte Carlo iterations to reach numerical convergence[21] to lower. The POF values displayed in Figure 8 correspond to those evaluated by a probabilistic criterion.
The influence of the outer coating shell thickness of the multicoated nePCMs, which is directly related to the number of ALD cycles (see Table 1), on the POF of the shells and the enthalpy decrease of the nePCMs is also studied, as shown in Figure 8. Notice that the values of melting enthalpy loss displayed in these Figures correspond to those experimentally obtained after 80 DSC cycles.
From Figure 8 a), the POF of the inner shell (SnO_2) of Sn@SnO_2@ SiO_2 remained almost constant regardless of the number of ALD cycles, while the POF of the outer shell (SiO_2) lowered with increasing outer shell thickness until a POF value of 72.38% was obtained for 50 ALD cycles. The constant inner shell trend (SnO_2) POF with its thickness did not affect mechanical reliability because the POF value was low. However, the POF of the SiO_2 coating lowered with an increasing number of ALD cycles; in absolute terms, the POF of the outer shell was still extremely high even for 50 ALD cycles. For melting enthalpy loss, a clear reduction was observed from when nePCMs were single-coated (null shell thickness) and when the extra coating was synthesised by ALD. However, the outer coating shell thickness did not strongly influence the evolution of this enthalpy loss. Therefore, all these results confirmed that although the SiO_2 coatings prevented nePCMs' enthalpy loss to some extent, their performance was still not optimal for them to be used in multicoated Sn nePCMs for energy storage purposes.
From Figure 8 b), it can be concluded that the POF of the inner shell (SnO) of Sn@SnO@Al_2O_3 did not notably change with the number of ALD cycles, but the outer shell (Al_2O_3) POF considerably reduced until a value of 1.66% for 50 ALD cycles. This sharp drop in the POF of the outer shell meant that Sn@SnO@Al_2O_3 would likely resist the thermal stresses that develop when undergoing thermal pro-

a) Sn@SnO

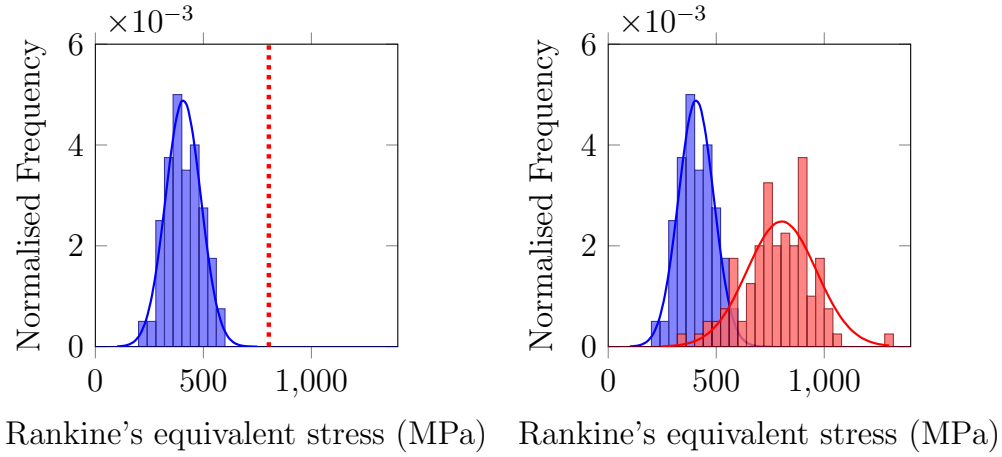

b) $Sn@SnO_2@SiO_2$

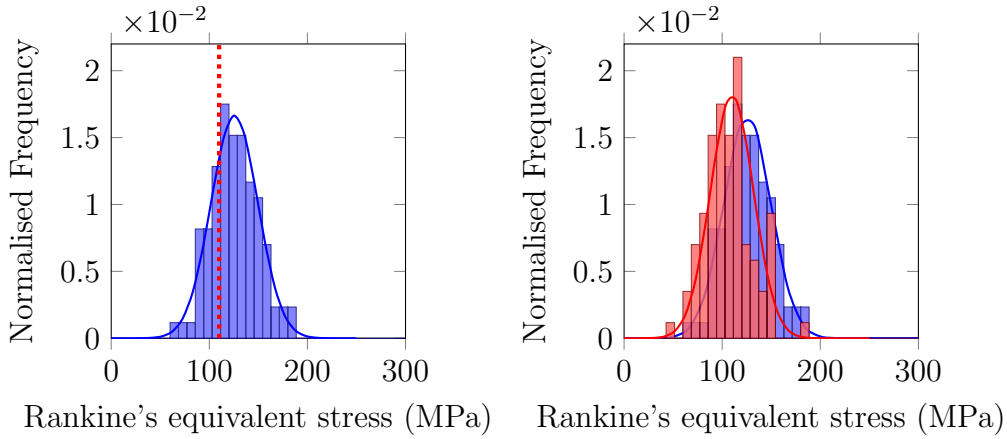

c) $Sn@SnO@Al_2O_3$

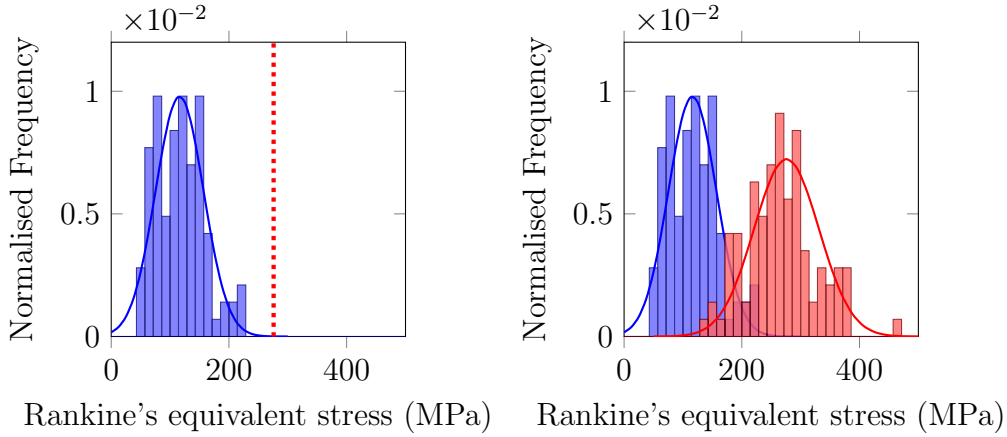

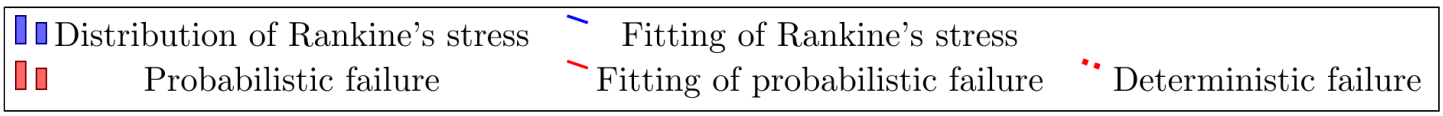

Figure 7: Deterministic (left) and probabilistic (right) failure criteria compared to maximum Rankine's equivalent stress obtained from the Monte Carlo simulation for the a) Sn@SnO, b) $Sn@SnO_2@SiO_2$ and c) $Sn@SnO@Al_2O_3$ nano-encapsulated phase change materials.

a) $Sn@SnO_2@SiO_2$

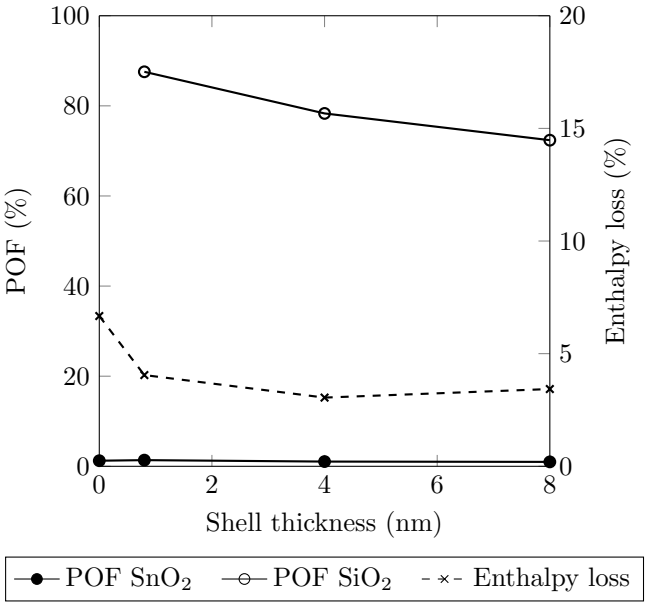

b) $Sn@SnO@Al_2O_3$

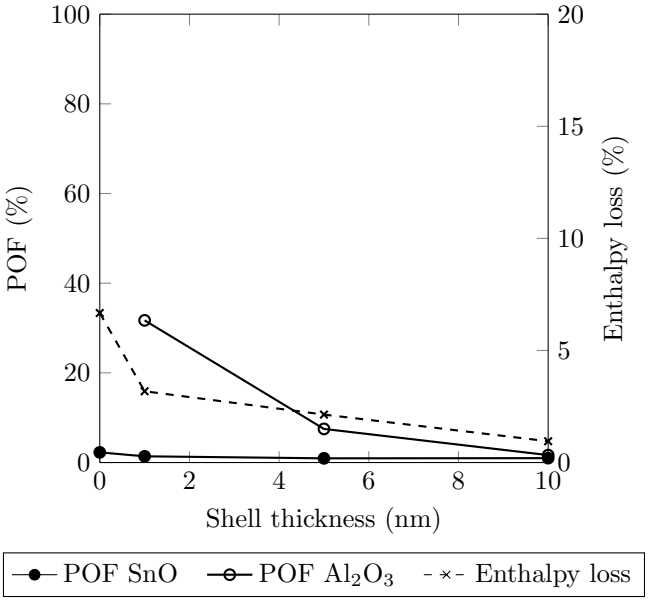

Figure 8: Evolution of the probability of failure (POF) of the inner and outer shells and of enthalpy loss with the outer shell thickness of the multicoated a) $Sn@SnO_2@SiO_2$ and b) $Sn@SnO@Al_2O_3$ nano-encapsulated phase change materials.

cesses. Furthermore, enthalpy loss significantly diminished to a value of 1.1% for 50 ALD cycles. Consequently, the good thermo-mechanical performance of Al_2O_3 makes it a good material candidate as a coating for multicoated nePCMs in energy storage applications.
Note that if SnO or SnO_2 were considered, the POF of these coatings was very low compared to the POF predicted for both SiO_2 and Al_2O_3 coatings, and there was no significant difference in the reliability between SnO and SnO_2 coatings. Thus, the oxidisation state of the tin oxide layer did not affect the multicoated nePCMs' thermal cycling performance. From a physical standpoint, the main parameters involved in nePCM mechanical failure were the thermal expansion coefficients of the core and shells, and the tensile strength of shells. More precisely, nePCMs were progressively heated until their core reached a liquid state to absorb energy, and the difference in the thermal expansion between both the core and shell was responsible for the thermal stresses that arose and would lead to shell mechanical failure. The larger the difference between the thermal expansion of the core and shell, the higher the thermal stress generated during heating cycles. The thermal expansion of Sn was 2×10^{-5} 1/K, while those of SiO_2 and Al_2O_3 were 5.7×10^{-7} 1/K and 8.2×10^{-6} 1/K, respectively. Hence, SiO_2 was more likely to undergo higher thermal stress than Al_2O_3. Furthermore, the difference in the mechanical failure between the Sn@SnO_2@SiO_2 and Sn@SnO@Al_2O_3 nePCMs was also influenced by the tensile strength of their outer shell materials: SiO_2 ($\sigma_t = 110$ MPa) and Al_2O_3 ($\sigma_t = 275.9$ MPa). Consequently, SiO_2 was less able to resist stress before its mechanical failure than Al_2O_3. Therefore, the combination of different tensile strengths, together with the difference in thermal expansion between nePCMs' cores and shells, help explain their different mechanical behaviour.
The present study offers an indirect experimental validation of the numerical results through their relation with nePCMs' enthalpy loss. There could be two different causes to explain why nePCMs lost enthalpy when undergoing thermal cycles: i) the nePCM core oxidation phenomena due to the atmosphere in which thermal cycling was conducted and oxygen diffusion through shell material pores; ii) the mechanical failure of the shell surrounding nePCM. As nePCM stability was assessed in an N_2 atmosphere, the first of the two reasons can be ruled out as the cause of nePCMs' enthalpy loss as oxidation could not take place. However, as shown in Figure 5, enthalpy loss still took place despite the fact that the experiment was conducted in an inert atmosphere. Thus, the only reason for this enthalpy loss in nePCMs was the mechanical failure of their shells, as also reported in a previous work by Navarrete et al.[12]. Therefore, the variation in nePCMs' enthalpy loss can be seen as an indirect experimental validation because enthalpy loss evolution with shell thickness (i.e. the number of ALD cycles) seems to agree with the drop in POF due to higher shell thickness values, which are the results predicted by the probabilistic numerical tool. Consequently, numerically predicting the POF of the multicoated nePCM outer shells in advance can contribute to reduce their enthalpy loss, which would have a direct impact on the energy storage performance of the application (nanofluids), from precisely tuning coating thickness by ALD.

6 Conclusions

This article presents a study about the mechanical reliability of experimentally synthesised multicoated nePCMs by applying a probabilistic numerical tool that combines MC methods with a FE thermo-mechanical model with phase change.
Starting with self-encapsulated Sn NPs, additional coatings were synthesised on nePCMs by the ALD technique to obtain multicoated nePCMs; i.e., Sn@SnO_2@SiO_2 and Sn@SnO@Al_2O_3. Their behaviour was experimentally characterised to study their thermal stability during heating cycles and to assess the stability of their phase change enthalpy with the outer shell thickness of the multicoated nePCMs, i.e. with the number of ALD cycles. The Al_2O_3 coatings better resisted thermal cycling than their SiO_2 counterparts. Regarding their mechanical performance, the Al_2O_3 coatings had a POF of only 1.66% after 50 ALD cycles, while the POF predicted for their SiO_2 coatings was of 72.38%. Furthermore, the POF of the outer shells is studied to assess the mechanical strength of the Sn@SnO, Sn@SnO_2@SiO_2 and Sn@SnO@Al_2O_3 nePCMs. Numerical predictions confirmed the experimental trend of the thicker the shell (and hence the more ALD cycles), the more marked the reduction in both the POF and phase

change enthalpy loss of nePCM cores. As an experimental characterisation of the multicoated nePCMs was performed in an N_2 atmosphere, oxidation was ruled out as the cause of the experimentally observed enthalpy loss of nePCM cores. Hence the reason for this enthalpy loss could only be nePCM shell mechanical failure. Furthermore, numerical simulations and thermal characterisation apparently indicated that the POF of outer shells and the enthalpy loss of nePCMs were related phenomena that could be used to validate the numerical tool.
In short, the coatings synthesised by ALD to obtain multicoated nePCMs enhanced their thermo-mechanical properties by precisely controlling outer shell thickness. Numerical simulations could be used to determine optimal coating thickness for a desired thermal energy storage application, which could contribute to reduce the coating cost of nePCMs and to better control nanofluid colloidal stability. Furthermore, the numerical tool herein used could be employed to make numerical predictions in an attempt to reduce the number of experiments to be run to mechanically characterise multicoated nePCMs.

Acknowledgements

This research was partially funded by the *Ministerio de Economía y Competitividad (MINECO)* of Spain through the Project ENE2016-77694-R. Josep Forner-Escrig thanks the *Ministerio de Economía, Industria y Competitividad* of Spain and Fondo Social Europeo for a pre-doctoral fellowship through Grant Ref. BES-2017-080217 (FPI program). Nuria Navarrete thanks the Universitat Jaume I (Spain) for a research mobility grant (Ref. E-2018-10) that enabled the experimental synthesis carried out in this article. This work was conducted by participants of the COST Action CA15119 Overcoming Barriers to Nanofluids Market Uptake (NANOUPTAKE).

References

[1] International Energy Agency. (IEA), *Solar energy perspectives*. Paris: International Energy Agency, 2011.

[2] B. Muñoz-Sánchez, J. Nieto-Maestre, I. Iparraguirre-Torres, A. García-Romero, and J. M. Sala-Lizarraga, "Molten salt-based nanofluids as efficient heat transfer and storage materials at high temperatures. an overview of the literature," *Renew. Sustain. Energy Rev.*, vol. 82, pp. 3924–3945, 2018.

[3] S. Choi and J. Eastman, "Enhancing thermal conductivity of fluids with nanoparticles," *Proceedings of the ASME International Mechanical Engineering Congress and Exposition, San Francisco, CA, USA*, 1995.

[4] S. Cingarapu, D. Singh, E. V.Timofeeva, and M. R. Moravek, "Nanofluids with encapsulated tin nanoparticles for advanced heat transfer and thermal energy storage," *Int. J. Energy Res.*, vol. 38, pp. 51–59, 2013.

[5] S. Cingarapu, D. Singh, E. V.Timofeeva, and M. R. Moravek, "Use of encapsulated zinc particles in a eutectic chloride salt to enhance thermal energy storage capacity for concentrated solar power," *Renew. Energy*, vol. 80, pp. 508–516, 2015.

[6] C. Liu, Z. Rao, J. Zhao, Y. Huo, and Y. Li, "Review on nanoencapsulated phase change materials: Preparation, characterization and heat transfer enhancement," *Nano Energy*, vol. 13, pp. 814–826, 2015.

[7] F. Rodríguez-Cumplido, E. Pabón-Gelves, and F. Chejne-Jana, "Recent developments in the synthesis of microencapsulated and nanoencapsulated phase change materials," *J. Energy Storage*, vol. 24, p. 100821, 2019.

[8] H. Xu, Z. Xing, F. Wang, and Z. Cheng, "Review on heat conduction, heat convection, thermal radiation and phase change heat transfer of nanofluids in porous media: Fundamentals and applications," *Chem. Eng. Sci.*, vol. 195, pp. 462–483, 2019.

[9] H. Xu and C. Zhao, "Analytical considerations on optimization of cascaded heat transfer process for thermal storage system with principles of thermodynamics," *Renew. Energy*, vol. 132, pp. 826–845, 2019.

[10] E. Alehosseini and S. M. Jafari, "Nanoencapsulation of phase change materials (PCMs) and their applications in various fields for energy storage and management," *Adv. Colloid Interface Sci.*, vol. 283, p. 102226, 2020.

[11] H.Xu, Y. Wang, and X. Han, "Analytical considerations of thermal storage and interface evolution of a pcm with/without porous media," *Int. J. Numer. Methods Heat Fluid Flow*, vol. 30, pp. 373–400, 2020.

[12] N. Navarrete, A. Gimeno-Furió, R. Mondragón, L. Hernández, L. Cabedo, E. Cordoncillo, and J. E. Juliá, "Nanofluid based on self-nanoencapsulated metal/metal alloys phase change materials with tuneable crystallisation temperature," *Sci Rep*, vol. 7, 2017.

[13] N. Navarrete, R. Mondragón, D. Wen, M. E. Navarro, Y. Ding, and J. E. Juliá, "Thermal energy storage of molten salt –based nanofluid containing nano-encapsulated metal alloy phase change materials," *Energy*, vol. 167, pp. 912 – 920, 2019.

[14] H. Peng, J. Wang, X. Zhang, J. Ma, T. Shen, S. Li, and B. Dong, "A review on synthesis, characterization and application of nanoencapsulated phase change materials for thermal energy storage systems," *Appl. Therm. Eng.*, vol. 185, p. 116326, 2021.

[15] S. S. Seyyed Afghahi and M. A. Golestani Fard, "Design and synthesis of a novel core-shell nanostructure developed for thermal energy storage purposes," *Ceram. Int.*, vol. 45, no. 13, pp. 15866–15875, 2019.

[16] S. Zhu, M. T. Nguyen, T. Tokunaga, and T. Yonezawa, "Size-Tunable Alumina-Encapsulated Sn-Based Phase Change Materials for Thermal Energy Storage," *ACS Appl. Nano Mater.*, vol. 2, no. 6, pp. 3752–3760, 2019.

[17] N. Navarrete, D. La Zara, A. Goulas, D. Valdesueiro, L. Hernández, J. R. van Ommen, and R. Mondragón, "Improved thermal energy storage of nanoencapsulated phase change materials by atomic layer deposition," *Sol. Energy Mater. Sol. Cells*, vol. 206, p. 110322, 2020.

[18] H. Van Bui, F. Grillo, and J. R. van Ommen, "Atomic and molecular layer deposition: off the beaten track," *Chem. Commun.*, vol. 53, pp. 45–71, 2017.

[19] J. Forner-Escrig, R. Palma, and R. Mondragón, "Finite element formulation to study thermal stresses in nanoencapsulated phase change materials for energy storage," *J. Therm. Stresses*, vol. 43, no. 5, pp. 543–562, 2020.

[20] J. Forner-Escrig, R. Mondragón, and R. Palma, "Mechanical Reliability of Core-Shell Nanoparticles for thermal energy storage by Finite Element Method," in *Conference Proceedings 1st Internationational Conference on Nanofluids (ICNf2019), 2nd European Symposium on Nanofluids (ESNf2019)*, pp. 258–261, Bubok Publishing S.L, 2019.

[21] J. Forner-Escrig, R. Mondragón, L. Hernández, and R. Palma, "Mechanical reliability analysis of nanoencapsulated phase change materials combining Monte Carlo technique and the finite element method," *Mech. Mater.*, vol. 158, p. 103886, 2021.

[22] M. D. McKay, R. J. Beckman, and W. J. Conover, "A comparison of three methods for selecting values of input variables in the analysis of output from a computer code," *Technometrics*, vol. 21, no. 2, pp. 239–245, 1979.

[23] J. van Ommen and A. Goulas, "Atomic layer deposition on particulate materials," *Mater. Today Chem.*, vol. 14, p. 100183, 2019.

[24] R. H. Perry, D. W. Green, and J. O. Maloney, *Perry's Chemical Engineers' Handbook*. New York: McGraw-Hill, 2008.

[25] *ASM Handbook Volume 2: Properties and Selection: Nonferrous Alloys and Special-Purpose Materials*. Materials Park: ASM International, 1990.

[26] F. Cverna, *ASM Ready Reference: Thermal Properties of Metals*. Materials Park: ASM International, 2002.

[27] S. V. Stankus and R. A. Khairulin, "The density of alloys of tin—lead system in the solid and liquid states," *High Temp.*, vol. 44, p. 389–395, 2006.

[28] M. J. Assael, A. Chatzimichailidis, K. D. Antoniadis, W. A. Wakeham, M. L. Huber, and H. Fukuyama, "Reference correlations for the thermal conductivity of liquid copper, gallium, indium, iron, lead, nickel and tin," *High Temp.-High Press.*, vol. 46, p. 391–416, 2017.

[29] *Landolt-Börnstein. Semiconductors. Non-Tetrahedrally Bonded Elements and Binary Compounds I*, vol. 41C. New York: Springer-Verlag Berlin Heidelberg, 1998.

[30] R. Gaillac and F.-X. Coudert, "ELATE elastic tensor analysis." http://progs.coudert.name/elate/mp?query=mp-856. Last Accessed: 21-10-2019.

[31] R. Gaillac, P. Pullumbi, and F.-X. Coudert, "Elate: an open-source online application for analysis and visualization of elastic tensors," *J. Phys. Condens. Matter*, vol. 28, no. 27, p. 275201, 2016.

[32] United States National Institutes of Health (NIH), "PubChem open chemistry database." https://pubchem.ncbi.nlm.nih.gov/compound/29011. Last Accessed: 21-10-2019.

[33] K. Nam, J. Wolfenstine, H. Choi, R. Garcia-Mendez, J. Sakamoto, and H. Choe, "Study on the mechanical properties of porous tin oxide," *Ceram. Int.*, vol. 43, pp. 10913–10918, 2017.

[34] MNX Mems & Nanotechnology Exchange, "MEMSnet®." https://www.memsnet.org/material/silicondioxidesio2film/. Last Accessed: 11-06-2020.

[35] Massachusetts Institute of Technology, "Thermal silicon oxide." http://www.mit.edu/ 6.777/matprops/sio2.htm. Last Accessed: 13-06-2020.

[36] Translume, "Fused silica material properties." https://www.translume.com/index.php/resources/item/186-fused-silica-material-properties. Last Accessed: 13-06-2020.

[37] W. M. Haynes, *CRC Handbook of Chemistry and Physics (92nd ed.).* Boca Raton: CRC Press, 2011.

[38] C. T. Lynch, ed., *Practical Handbook of Materials Science.* Boca Raton: CRC Press, 1989.

[39] J. F. Shackelford, Y.-H. Han, S. Kim, and S.-H. Kwon, *CRC Materials Science and Engineering Handbook, Fourth Edition.* Boca Raton: CRC Press, 2015.

[40] Accuratus Corporation, "Aluminum oxide, Al_2O_3 ceramic properties." https://accuratus.com/alumox.html. Last Accessed: 18-08-2019.

[41] K. Persson, "Materials Data on SnO (SG:129) by Materials Project," 2014. https://materialsproject.org/materials/mp-2097/. Last Accessed: 10-08-2020.

[42] K. Persson, "Materials Data on SnO2 (SG:136) by Materials Project," 2014. https://materialsproject.org/materials/mp-856/. Last Accessed: 10-08-2020.

[43] Massachusetts Institute of Technology (MIT), "Thermal silicon oxide." http://www.mit.edu/ 6.777/matprops/sio2.htm. Last Accessed: 11-08-2020.

[44] R. E. Melchers and A. T. Beck, *Structural Reliability Analysis and Prediction, 3rd Edition.* New York: John Wiley & Sons, Ltd., 2018.